Volume 13
Number 4
April 2026
Pages 1743–2152

Environmental Science Nano

rsc.li/es-nano

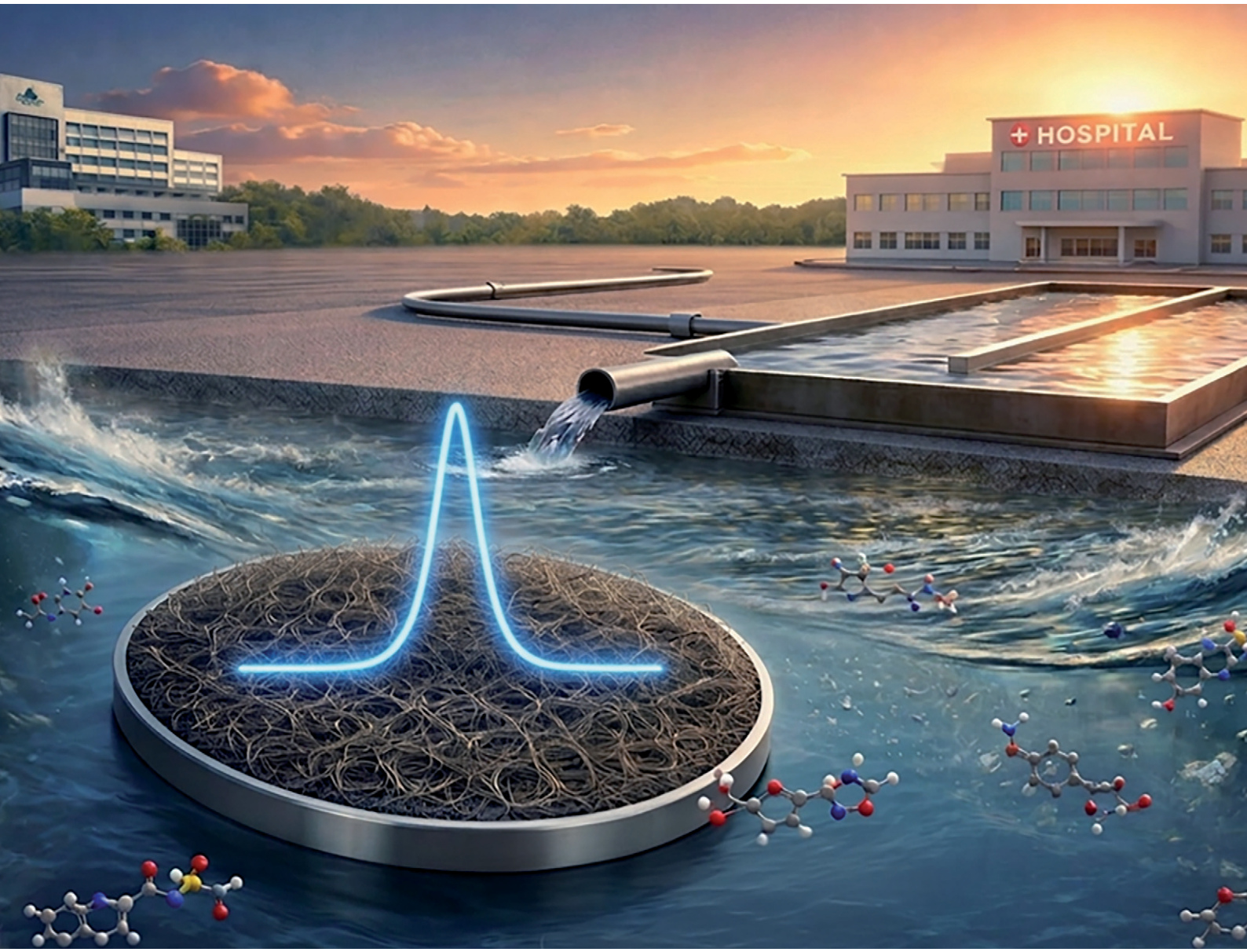

ISSN 2051-8153

ROYAL SOCIETY OF CHEMISTRY

PAPER

Paulina Sierra-Rosales, José Miguel González-Domínguez *et al.*
Electrochemical detection of sulfamethoxazole in water matrices using green nanomaterials: pilot-scale validation in a solar photo-Fenton process

Environmental Science Nano

ROYAL SOCIETY OF CHEMISTRY

PAPER

View Article Online
View Journal | View Issue

Cite this: *Environ. Sci.: Nano*, 2026, **13**, 1896

Electrochemical detection of sulfamethoxazole in water matrices using green nanomaterials: pilot-scale validation in a solar photo-Fenton process

Víctor Calvo, [a] Constanza J. Venegas, [b] Paulina Sierra-Rosales, *[c] Sara Miralles-Cuevas, [de] Alejandro Cabrera-Reina, [de] Wolfgang K. Maser, [a] Ana M. Benito [a] and José Miguel González-Domínguez *[a]

Received 30th January 2026,
Accepted 5th March 2026

DOI: 10.1039/d6en00086j

rsc.li/es-nano

This work presents an electrochemical sensor designed as a process-monitoring tool for tracking sulfamethoxazole (SMX) during advanced oxidation processes (AOPs) under pilot-scale, realistic wastewater conditions. The sensor is based on eco-friendly aqueous inks combining carbon nanomaterials with nanostructured biopolymers, specifically carbon nanofibers with cellulose nanocrystals (CNF/CNC) or multi-walled carbon nanotubes with chitin nanocrystals (CNT/ChNC), which were deposited onto glassy carbon electrodes (GCEs) to enhance the electrochemical response toward SMX. Among the tested configurations, the CNF/CNC-based sensor exhibited the best performance for SMX monitoring in the mg L^{-1} concentration range, combining a wide linear response and a detection limit of 0.17 mg L^{-1} with robust, reproducible behavior. Sensor calibration and performance were evaluated in both ultrapure water and synthetic hospital wastewater, highlighting the impact of matrix effects while confirming reliable operation under complex conditions. Crucially, the sensor was validated during the monitoring of SMX degradation in a pilot-scale solar photo-Fenton process operated at circumneutral pH using Fe^{3+}-EDDS as a catalyst, with electrochemical measurements showing excellent agreement with UHPLC-DAD reference analyses (Pearson's $r > 0.99$). Rather than targeting ultra-trace detection, this study demonstrates the potential of electrochemical sensing as a rapid, cost-effective, and near-real-time tool for process monitoring and control in high-load effluents, such as hospital and pharmaceutical wastewater. These results bridge the gap between laboratory-scale sensor development and operational wastewater treatment applications, highlighting the relevance of sustainable nanocarbon–biopolymer inks for real-world environmental monitoring.

Environmental significance

Emerging contaminants in wastewater represent a growing environmental challenge due to their persistence and potential health risks. Traditional detection methods are often costly, complex, or environmentally harmful. This study introduces an eco-friendly electrochemical sensor using carbon nanomaterials dispersed with biobased nanocrystals (cellulose or chitin), without toxic solvents and surfactants. Validated under realistic conditions, including pilot-scale solar photo-Fenton treatment, the sensor enables real-time, scalable monitoring of pollutants. Its green fabrication and operational simplicity make it suitable for decentralized water quality control. By enhancing contaminant detection through green materials and methods, this work supports safer water reuse and contributes directly to UN Sustainable Development Goal 6 (Clean Water and Sanitation), promoting access to clean water through innovative and sustainable technologies.

1. Introduction

Contaminants of emerging concern (CECs) have garnered increasing scientific and regulatory attention due to their persistence in the environment and potential risks to public health. In a world facing growing water scarcity, water reuse has become a strategic necessity, making the effective removal of CECs a critical priority. These contaminants include pharmaceuticals, pesticides, industrial chemicals, and other bioactive synthetic compounds.[1,2] Although specific regulations for CECs remain limited globally,

[a] *Instituto de Carboquímica (ICB-CSIC), C/Miguel Luesma Castán 4, Zaragoza, Spain. E-mail: jmgonzalez@icb.csic.es*
[b] *Departamento de Química Inorgánica y Analítica, Facultad de Ciencias Químicas y Farmacéuticas, Universidad de Chile, Olivos 1007, Independencia, Santiago, Chile*
[c] *Instituto Universitario de Investigación y Desarrollo Tecnológico (IDT), Universidad Tecnológica Metropolitana (UTEM), Santiago, Chile. E-mail: psierra@utem.cl*
[d] *Solar Energy Research Centre (CIESOL), Joint Centre University of Almería-CIEMAT, Ctra. de Sacramento s/n, 04120, Almería, Spain*
[e] *Chemical Engineering Department, University of Almería, Ctra. de Sacramento s/n, 04120, Almería, Spain*

initiatives have been developed to address their environmental impact. Notably, the European Union has implemented regulatory strategies since the early 2000s, targeting municipal wastewater treatment plants (MWWTPs) as major pathways for CEC release into aquatic ecosystems, along with pharmaceutical and hospital effluents.

The recently adopted European Directive 2024/3019 introduces a significant regulatory shift by mandating quaternary treatment stages to remove micropollutants and emphasizing comprehensive monitoring of other CECs, including antibiotic resistance genes (ARGs), per- and polyfluoroalkyl substances (PFAS), microplastics, and toxic disinfection by-products (DBPs).[3] Furthermore, the enforcement of the "polluter pays" principle directly impacts sectors such as the pharmaceutical industry and hospitals, highlighting the need for advanced treatment and monitoring solutions.

Hospital wastewater is recognized as a particularly relevant source of pharmaceutical contamination, often containing significantly higher concentrations of certain drugs than MWWTP effluents. Several studies have reported substantial loads of antibiotics and other pharmaceuticals in hospital discharges, raising concerns about their direct release into receiving waters or their dilution and dissemination through centralized treatment facilities.[4–7] In this context, decentralized or source-based treatment strategies, coupled with monitoring tools that track contaminant concentration dynamics, are increasingly considered essential to prevent the uncontrolled spread of these compounds. Among pharmaceuticals of concern, antibiotics are widely recognized as an imminent threat to public health, a concern strongly emphasized by the World Health Organization (WHO). Sulfamethoxazole (SMX), a broad-spectrum antibiotic extensively used in both human and veterinary medicine, has emerged as a prominent model CEC due to its frequent detection in surface water, groundwater, and MWWTP effluents.[8] Reflecting its environmental prevalence and potential health risks, SMX has been included in the updated EU watch list for priority monitoring.[9,10] Moreover, SMX is commonly employed as a referent pollutant in studies aimed at developing and evaluating advanced oxidation processes (AOPs), given its recalcitrant nature and representative behavior among sulfonamide antibiotics.[11–15] Conventional water treatment processes are often insufficient for effectively removing CECs, underscoring the need for innovative, sustainable treatment approaches.[16] AOPs, which generate highly reactive, non-selective species such as hydroxyl radicals (HO·), have attracted increasing attention as effective strategies for degrading persistent organic contaminants and inactivating microorganisms.[17] Among them, the solar photo-Fenton process, which uses iron salts and H_2O_2, stands out due to its cost-effectiveness and high degradation efficiency.[15,18] Recent research efforts have focused on improving the scalability and economic feasibility of this process, with raceway pond reactors demonstrating their viability at pilot and demonstration scales.[19–22] In parallel, increasing attention has been paid to process control and optimization, including the monitoring of key operational parameters and reagents such as H_2O_2.[23–27] These developments highlight the need for sensing tools capable of tracking not only treatment reagents but also recalcitrant model CECs, which can serve as performance indicators during advanced oxidation treatments.

Ultra-high-performance liquid chromatography (UHPLC) remains the gold standard for the detection and quantification of CECs due to its high sensitivity, low detection limits, and analytical reliability. However, UHPLC-based methods are inherently expensive and time-consuming, requiring complex sample preparation and lengthy analysis times, which limit their suitability for on-site or near-real-time applications. In contrast, electrochemical sensors have emerged as a promising alternative, offering rapid analysis, operational simplicity, and compatibility with *in situ* or on-site monitoring in complex environmental matrices.[26–28] By converting chemical information into electrical signals, electrochemical sensors provide timely feedback, particularly valuable for process monitoring and control applications.[29,30]

In recent years, unidimensional carbon nanomaterials (CNMs), such as carbon nanotubes (CNTs) and carbon nanofibers (CNFs), have attracted considerable attention for electrochemical sensing applications due to their high surface area, excellent electrical conductivity, and chemical stability.[31,32] Nevertheless, conventional CNM processing often relies on unsustainable surfactants or organic solvents, which can induce aggregation, structural degradation, and compromised electrochemical performance.[31,33]

Nanostructured biopolymers (NBs) offer a sustainable alternative, enabling water-based processing of CNMs while preserving their functional properties.[34–38] Biopolymers such as cellulose nanocrystals (CNCs) and chitin nanocrystals (ChNCs), derived from renewable sources, provide colloidal stability, biocompatibility, and eco-friendly dispersibility. CNCs, obtained from cellulose, the most abundant biopolymer on Earth, have been shown to enhance CNM dispersibility in aqueous media[36,37] and to improve electrochemical sensor performance, particularly selectivity and sensitivity.[38] The crystalline structure of CNCs plays a critical role in electroanalytical outcomes, with type II CNC-based inks achieving up to 20-fold higher sensitivity in glycoprotein detection.[38] ChNCs, derived from chitin, the second most abundant biopolymer, exhibit electropositive surface charges that further promote CNM dispersion.[39–41] Despite their demonstrated potential as green dispersants,[36] the application of ChNCs in electrochemical sensing remains largely unexplored.

Despite the extensive literature on electrochemical sensors for SMX and related pharmaceuticals, most reported systems have been developed primarily to achieve ultra-low detection limits under static, idealized laboratory conditions, typically using ultrapure water or simple buffer solutions. While such

approaches are well-suited for trace-level environmental analysis, they are not necessarily designed to operate under the dynamic, chemically complex conditions encountered in wastewater treatment processes. In operational scenarios involving hospital or pharmaceutical effluents, where SMX concentrations are often orders of magnitude higher than in urban wastewater, the key analytical requirements shift toward robustness, tolerance to matrix effects, and the ability to provide rapid feedback on concentration dynamics rather than ultra-trace sensitivity.

In this context, the present work addresses this gap by evaluating two eco-friendly, fully water-processed CNM-based inks stabilized with nanostructured biopolymers, CNF/CNC and CNT/ChNC, for the development of electrochemical sensors targeting SMX monitoring. To the best of our knowledge, this is the first study to systematically compare these two CNM/NB hybrid ink formulations for SMX electrochemical monitoring within the framework of advanced wastewater treatment research. Beyond laboratory-scale evaluation, the best-performing sensor is validated under near-real operational conditions, including measurements in complex synthetic hospital wastewater and, critically, the monitoring of SMX degradation during a pilot-scale solar photo-Fenton process, with direct cross-validation against UHPLC-DAD. By explicitly targeting process monitoring rather than trace analysis, this work aims to bridge the often-overlooked gap between laboratory sensor development and operational wastewater treatment applications.

2. Materials and methods

2.1. Reagents

Microcrystalline cellulose powder (20 μm (#310697)), chitin extracted from shrimp shells (practical grade, powder; C7170), concentrated H_2SO_4, monobasic potassium phosphate (KH_2PO_4, 99%), and dibasic potassium phosphate (K_2HPO_4, 98%) were purchased from Sigma-Aldrich (Spain). Potassium chloride (KCl), potassium ferrocyanide ($K_4Fe(CN)_6{\cdot}H_2O$, 98.5–102.0%), and potassium ferricyanide ($K_3Fe(CN)_6$, 99%) were obtained from Merck. Hydrochloric acid 37% (AGR IS CHAC-0AI) was purchased from Labkem. Ultrapure water, purified using a Siemens Ultraclear device, was used throughout all the experimental procedures to prepare the nanomaterials and the dispersions. CNFs were supplied by ASI (Pyrograf® III PR 24 LHTXT) and were produced by chemical vapor deposition (CVD). MWCNTs were purchased from Nanocyl (NANOCYL NC 7000™) and synthesized using catalytic CVD. MWCNTs were slightly oxidized to enhance their interaction with ChNCs, following the methodology described in our recent publication.[42] See the SI for the comparison of the characterization results of both CNMs (Fig. S1). SMX (>99%) and ethylenediamine-*N*,*N*′-disuccinic acid (EDDS) (35% w/v) were supplied by Sigma Aldrich (Chile). EDDS was used as an iron complexing agent to enable the photo-Fenton process to operate at circumneutral pH. The reagents used as eluents for SMX quantification by UHPLC-DAD were formic acid (95%, w/v) and HPLC-grade acetonitrile, both purchased from Sigma-Aldrich (Chile). The reagents used as eluents for Fe^{3+}-EDDS quantification were sodium formate (>99%, w/w), tetra-*n*-butylammonium hydrogen sulfate (>99%, w/w), and HPLC-grade methanol. Ferric sulfate ($Fe_2(SO_4)_3{\cdot}H_2O$, 97% w/w) used as an Fe^{3+} source and the reagents for iron quantification consisting of *ortho*-phenanthroline (99%, w/w), glacial acetic acid (>99%, w/v), and ascorbic acid (99%, w/w) were also supplied by Panreac (Chile). Titanium(IV) oxysulfate solution (1.9%, w/v) was used for H_2O_2 quantification, and H_2O_2 (33% w/v) was provided by Farmalatina (Chile). All reagents needed to prepare the synthetic hospital wastewater (see section 2.3) were purchased from Alquimistas Ltda. and Farmalatina Ltda. (Chile). All solutions were prepared using ultrapure water generated by a Milli-Q® water purification system (model PURELAB Option Q-7), which has a specific resistance of 18.2 MΩ cm.

2.2. Synthesis and characterization of nanomaterials

Synthesis of CNCs. Type II CNCs were synthesized according to a protocol developed in our research group for controlling the allomorph outcome, as published in our paper.[43] Detailed synthesis procedures and characterization results are provided in the SI.

Synthesis of ChNCs. ChNCs were prepared by an adapted method of acid hydrolysis with hydrochloric acid.[42,44] Full details on the synthesis protocol and characterization results are provided in the SI.

Preparation of the CNM/NB inks. The optimization of a combination of CNFs and CNCs was previously reported in a publication.[37] The optimized method used type II CNCs and CNFs at a concentration of 3 g L^{-1}, employing ultrasonication, centrifugation, and redispersion. Additionally, the optimization of the MWCNT and ChNC combination was also detailed in another recent publication.[42] In summary, 1 g L^{-1} MWCNTs were combined with 3.5 g L^{-1} ChNCs in ultrapure water, using an ultrasound tip to induce the interaction. The dispersions were centrifuged at 4000 rpm (1842 rcf) for 4 min to remove non-dispersed materials.

Characterization of the CNM/NB inks. Diluted samples of the CNM/NB inks were subjected to UV-vis spectroscopy using a Shimadzu UV-2401PC spectrophotometer before and after centrifugation to estimate the CNM concentration. Absorbance measurements for MWCNT/ChNC inks were taken at 850 nm, while those for CNFs were taken at 650 and 700 nm. Subsequently, the inks were characterized using dynamic light scattering (DLS) and ζ-potential analysis on a Malvern Nano ZS instrument, with carbon reference parameters employed. The inks were lyophilized, and the solids were analyzed by XRD, TGA, and Raman spectroscopy.

Modification of glassy carbon electrodes. Glassy carbon electrodes (GCEs, CH Instruments, 3.0 mm in diameter) were

polished using 0.3 and 0.05 μm alumina powder (Leco) and rinsed with deionized water. The CNM/NB inks were drop-cast onto the polished GCEs, forming a homogeneous film. The modification process involved two repetitions of depositing 5 μL of the ink, followed by drying at 60 °C in an oven. Two CNM concentrations (0.2 and 0.4 g L^{-1}) of the CNM/NB inks were evaluated.

Morphological and structural analysis. XRD analysis was conducted using a Bruker D8 Advance diffractometer in the Bragg–Brentano geometry in the range of 2θ = (5–40°), with a step size of 0.05° and an accumulation time of 3 seconds. TGA measurements were performed using a Netzsch TG 209F1 device under a N_2 atmosphere, with a heating rate of 10 °C min^{-1} from room temperature to 800 °C. Raman spectroscopy was performed using a dispersive micro-Raman LabRam HR800 UV device (Horiba Jobin Yvon), equipped with a 532 nm excitation laser, a CCD detector, and a confocal microscope. Additionally, scanning electron microscopy (SEM) images were obtained using a Gemini 360 ZEISS field-emission microscope at 5.0 kV after preparing thin films using the same procedure as for modifying the glassy carbon electrodes, but on glassy carbon disks.

Electrochemical characterization of the sensor. Electrochemical measurements were performed on a CHI650E potentiostat (CH Instruments) using a three-electrode configuration. Bare and modified glassy carbon electrodes were used as working electrodes; the reference electrode utilized was Ag/AgCl (3.0 M KCl), while a platinum wire served as the counter electrode. A supporting electrolyte solution consisting of 0.1 M phosphate buffer solution (PBS) (pH = 7.4) with 0.1 M KCl was employed. The modified electrodes were first evaluated by cyclic voltammetry (CV) using 5 mM $[Fe(CN)_6]^{4-/3-}$ prepared in the supporting electrolyte. The CV parameters were a scan potential range of −0.1 V to 0.6 V, a scan rate of 50 mV s^{-1}, and an equilibrium time of 2 seconds.

SMX detection optimization using an electrochemical sensor. The optimization of the CNM/NB ink concentration and accumulation time was performed using differential pulse voltammetry (DPV), with a potential range of 0.4 V to 1.6 V, an amplitude of 0.05 V, and a pulse width of 0.06 s with a solution containing a known concentration of SMX in a buffer solution of 0.1 M KCl and 0.1 M PBS. The accumulation time represents the duration of contact between the solution and the modified electrode before the measurement. Measurements were conducted over a range of SMX concentrations (1–100 mg L^{-1}) to obtain a calibration curve and determine the linear detection range in ultrapure water. For the synthetic hospital wastewater matrix, the measurements were conducted over a range of SMX concentrations (1–30 mg L^{-1}). The results were processed using Origin software, fitting the data to a line and using the slope (b) and the standard error of the intercept on the y-axis (d_s) to estimate the detection limit (LOD) according to eqn (1).

$$\mathrm{LOD} = \frac{3d_s}{b} \quad (1)$$

2.3. Water matrix under study

To validate the proposed method for SMX determination, the SMX concentration was simultaneously monitored using both UHPLC-DAD and the sensor during various assays in which SMX was degraded by the photo-Fenton process. This validation was performed in a complex matrix comprising organic and inorganic compounds selected to simulate real-world conditions, specifically those present in hospital effluents, where pharmaceutical concentrations are usually higher than those in MWWTP effluents. The synthetic recipe, adapted from a previous publication by Zhang *et al.*,[45] was composed of the following inorganic components: $CaSO_4{\cdot}2H_2O$ (60 mg L^{-1}), $MgSO_4$ (60 mg L^{-1}), KCl (500 mg L^{-1}), $(NH_4)_2SO_4$ (24 mg L^{-1}), K_2HPO_4 (7.0 mg L^{-1}) and $NaHCO_3$ (105 mg L^{-1}); organic components: beef extract (1.8 mg L^{-1}), peptone (2.7 mg L^{-1}), humic salts (4.2 mg L^{-1}), sodium lignin sulfonate (2.4 mg L^{-1}), sodium lauryl sulfate (0.9 mg L^{-1}), acacia gum powder (4.7 mg L^{-1}), and arabic acid (5.0 mg L^{-1}).

2.4. Validation procedure: solar photo-Fenton experiments

The solar photo-Fenton process, mediated with EDDS as an iron complexing agent, was selected to validate the sensor measurement during a wastewater degradation treatment. The solar photo-Fenton process, particularly when operating at near-neutral pH, is considered one of the most efficient methods for removing CECs.[46–48] This process was implemented at a pilot plant scale in a low-cost raceway pond reactor[49] with a total volume of 19 L and 5 cm liquid depth (optical path length). This system consists of extensive channels through which a paddle wheel recirculates water. Operational conditions were selected based on previous studies, specifically using 0.10 mM Fe^{3+} with a 1 : 1 molar ratio of Fe^{3+}-EDDS and 1.5 mM H_2O_2.[14]

The experimental procedure involves preparing the synthetic matrix 24 hours before the experiments. This solution was placed in the raceway pond reactor in the dark, where SMX was first added, followed by the Fe^{3+}-EDDS complex. H_2O_2 was then added simultaneously with the uncovering of the photo-reactor, marking the start of the solar photo-Fenton reaction. Duplicate samples were collected at various time points during the 60 minute experiments to monitor the SMX concentration using UHPLC-DAD and the proposed electrochemical sensor. The Fe^{3+}-EDDS concentration was also measured by UHPLC-DAD, along with the H_2O_2 concentration, temperature, and other key parameters for process efficiency and control.

Regarding the UHPLC determination (Thermo Scientific Vanquish Core), a linear gradient was employed for SMX analysis, starting with 10% acetonitrile (A) and 90% HPLC-grade water containing 25 mM formic acid (B), and culminating in 100% B after 13 minutes. The re-equilibration time lasted 3 min. The retention time for SMX was 8.62 ± 0.01 min, with a quantification wavelength of 267 nm. The concentration of

Fe^{3+}-EDDS was also monitored *via* UHPLC-DAD in the same system, following the protocol outlined by Wu *et al.*[50] The mobile phase consisted of 5% methanol (A) and 95% buffer containing 15 mM sodium formate and 2 mM tetrabutylammonium hydrogen sulfate, adjusted to pH 4 with acetic acid (B). The retention time was 6.71 ± 0.05 min, with the quantification wavelength at 240 nm. The concentration of H_2O_2 was analyzed using a spectrophotometric method based on its reaction with titanium(IV) oxysulfate, as specified in DIN 38402H15 (measured at 410 nm).

All electrochemical measurements were performed in a fixed-volume electrochemical cell with a total volume of 10 mL. For each experiment involving samples collected from the pilot-scale reactor, 9.0 mL of the reactor effluent was directly transferred to the electrochemical cell, and the remaining 1.0 mL was completed with the supporting electrolyte (0.1 M PBS + 0.1 M KCl). This procedure ensured constant ionic strength and pH conditions. Differential pulse voltammetry measurements were performed after the specified accumulation time. The concentration of SMX in the pilot-scale samples was determined from the measured peak current using an external calibration curve previously constructed in synthetic hospital wastewater under identical electrochemical conditions.

3. Results and discussion

3.1. Characterization of CNM/NB inks and electrodes

Two nanomaterial-based aqueous inks, comprising CNF/CNC and CNT/ChNC, were successfully prepared and characterized. The inks were previously optimized to maximize the CNM concentration while ensuring stability for electrode modification.[37,42] Their characterization is summarized in Table 1 and Fig. 1. The CNF/CNC ink exhibits a larger hydrodynamic radius compared to the CNT/ChNC ink, reflecting the inherently larger size of CNFs, yet maintains a lower polydispersity index (Table 1). The CNT/ChNC ink shows a positive ζ-potential, attributed to protonated residual amino groups on the ChNCs. In contrast, the CNF/CNC ink presents a negative ζ-potential due to the existence of sulfonated hydroxyl groups on the nanocellulose surface. Notably, the absolute ζ-potential values are comparable for both inks, indicating similar dispersion stability over time, likely maintained through electrostatic repulsions.

The XRD profiles (Fig. 1A) of the CNM/NB inks retain the characteristic peaks of their respective nanobiopolymers (NBs), while also displaying the prominent (002) graphitic plane associated with the carbon nanomaterials. In the CNT/ChNC hybrid, this peak overlaps with the (013) peak of the ChNCs, whereas in the CNF/CNC hybrid, the (002) peak is more pronounced, reflecting the higher CNM concentration (Table 1) and a greater degree of graphitization in the CNFs. The Raman spectra of the hybrids (Fig. 1B) closely match those of the pure CNMs (Fig. S1B), exhibiting the two characteristic bands: the G band (~1580 cm^{-1}), related to the degree of graphitization, and the D band (~1340 cm^{-1}), which arises from disorder in the sp^2 carbon network. NBs are not detected in the Raman spectra of the hybrids, likely due to their weak Raman response and the strong resonance of CNMs. The thermal degradation profiles of the inks (Fig. 1C) reveal notable differences: the CNT/ChNC ink exhibits higher thermal resistance, as indicated by its higher degradation onset temperature and lower residue compared to the CNF/CNC material. Considering the high thermal intrinsic stability of CNMs under N_2 and the minimal residue contributed by NBs, these results suggest a relatively higher CNM content in the CNF/CNC hybrid.

Both CNM/NB inks were used to modify glassy carbon electrodes (GCEs) at two CNM concentrations (0.2 and 0.4 g L^{-1}). Their electrochemical performance was evaluated *via* cyclic voltammetry using $[Fe(CN)_6]^{4-}/[Fe(CN)_6]^{3-}$ as a redox mediator (Fig. 1D). The bare GCE served as a reference, confirming its intrinsic electrochemical activity and the redox mediator's reversible behavior. All the modified electrodes exhibited enhanced electrochemical responses compared to the bare GCE, with the CNT/ChNC-modified electrode showing the highest peak currents. This could be related to the surface charges of the modified electrodes. The CNT/ChNC electrode exhibits the best electrochemical response to the negative redox mediator due to the film's positive charge, whereas the CNF/CNC ink electrode exhibits a negative charge. These charges interact with the redox mediator, generating distinct current responses between the modified electrodes. In addition, increasing the CNM concentration from 0.2 to 0.4 g L^{-1} further enhanced the current response for both hybrid inks, highlighting the effect of CNM loading on the electrode performance (Table S1). Based on the mean current values and their standard deviation, the coefficient of variation (CV, %) for each electrode was calculated. As shown in Table S1, the GCE is highly reproducible due to its mirror-like surface (CV of 1.1%), which is associated with a homogeneous surface. For modified electrodes, the CV percentage is always higher than that of the bare electrode due to the incorporation of errors inherent to the new surface. Table S1 shows that the modified electrodes exhibit high CV percentages, but all have a coefficient of

Table 1 Characterization of the CNM/NB aqueous colloids. Parameters include CNM concentration (determined by UV-vis spectroscopy), hydrodynamic radius, polydispersity index, and ζ-potential

CNM/NB ink	CNM concentration (g L^{-1})	Hydrodynamic radius (nm)	Polydispersity	ζ-Potential (mV)
CNF/CNC	0.80	236 ± 6	0.32 ± 0.04	−18 ± 1
CNT/ChNC	0.41	118 ± 9	0.44 ± 0.05	21 ± 1

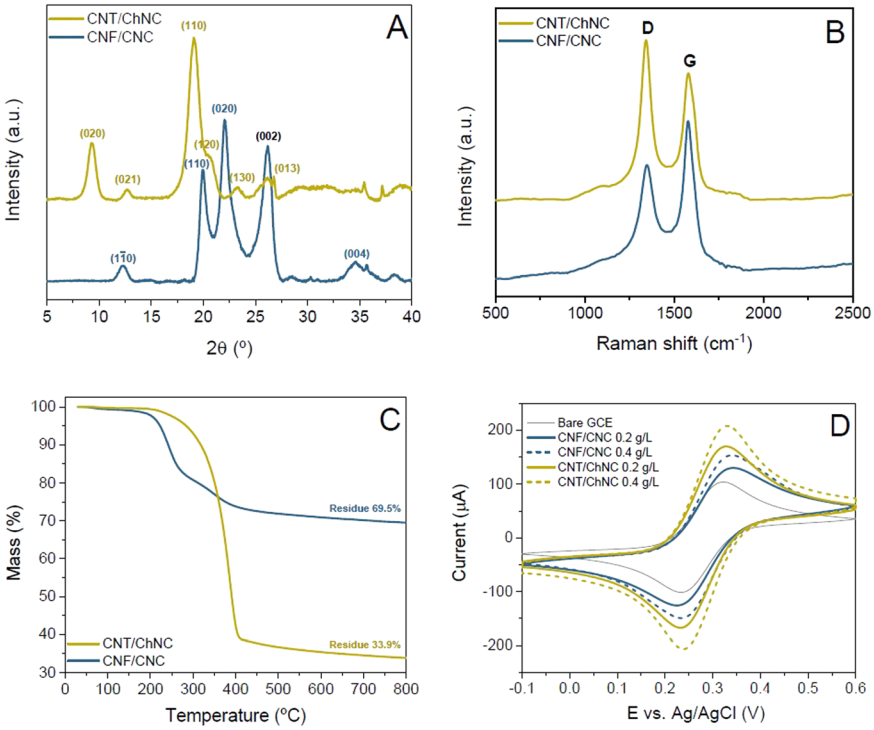

Fig. 1 (A) XRD patterns of lyophilized inks; (B) Raman spectra of lyophilized inks; (C) thermogravimetric analysis of lyophilized inks under a N_2 atmosphere; (D) cyclic voltammograms of glassy carbon electrodes modified with each ink in 5 mM $K_3Fe(CN)_6/K_4Fe(CN)_6$ and 0.1 M PBS + 0.1 M KCl. Solid lines: 0.2 g L^{-1}; dotted lines: 0.4 g L^{-1}. The bare GCE is shown as a black solid line for reference.

variation less than 5%, except for CNT/ChNC 0.2 g L^{-1} (7.8%). In any case, the values of the coefficient of variation obtained are low, which indicates that the films formed on the electrode are homogeneous and the sensors, therefore, are reproducible. These results confirm that the electrodes modified with 0.4 g L^{-1} are the most suitable for the next experiments.

FESEM images (Fig. 2) reveal notable morphological differences between carbon films deposited from the CNF/CNC and CNT/ChNC inks onto glassy carbon electrodes. The CNF/CNC film (Fig. 2A and B) displays a more exposed surface and higher porosity, whereas the CNT/ChNC film (Fig. 2C and D) forms a denser

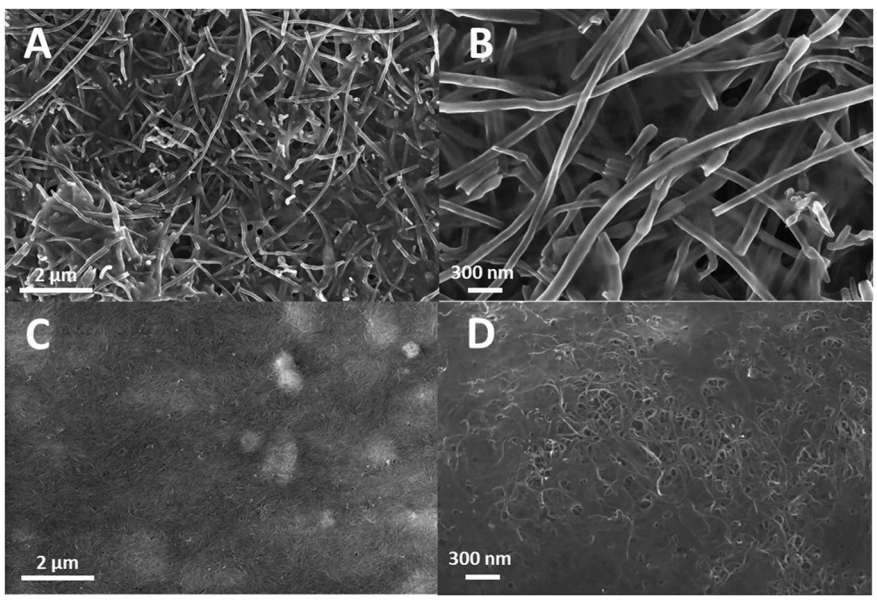

Fig. 2 FESEM images of the CNM/NB films over glassy carbon disks after drop casting 0.4 g L^{-1} inks: CNF/CNC (A and B) and CNT/ChNC (C and D).

network, with ChNCs surrounding the CNTs. The size disparity between the CNMs is also evident, with CNFs appearing longer and broader than CNTs. It is important to note that a more homogeneous film on the electrode will improve the reproducibility of the sensors.

3.2. Optimization of the SMX quantification by electrochemistry

SMX was quantified using differential pulse voltammetry (DPV), a highly sensitive technique widely applied for the electrochemical determination of trace analytes.[51,52] The initial DPV measurements (Fig. 3A) performed with 100 mg L^{-1} SMX revealed a pronounced electrocatalytic effect at the CNT/ChNC-modified electrodes, evidenced by a peak potential shift of ~0.1 V relative to both the bare GCE and the GCE/CNF/CNC-modified electrodes. In addition, both CNF/CNC and CNT/ChNC hybrids exhibited a clear concentration-dependent enhancement of the electrochemical signal, with the CNT-based electrodes consistently delivering higher current responses at equivalent CNM concentrations. Interestingly, at the higher concentration (0.4 g L^{-1}), the current difference between the two hybrids decreases, suggesting similar electrochemical performance under these conditions. Overall, these results confirm the ability of CNM/NB inks to significantly enhance electrochemical monitoring of SMX, reinforcing their potential for sensitive, reliable monitoring of contaminants in environmental samples.

To improve the response and reproducibility of SMX detection, the accumulation time was optimized for electrodes modified with CNM/NB inks at 0.4 g L^{-1} (Fig. 3B). Accumulation times from 0 to 4 minutes were tested to preserve a rapid analytical process. For the CNF/CNC-modified electrodes, increasing the accumulation time beyond 1 minute did not significantly enhance the current response, likely because the electrode surface saturated rapidly. Consequently, an accumulation time of 1 minute was selected as optimal, as it provided both reproducibility and minimal experimental duration. In contrast, electrodes modified with the CNT/ChNC ink exhibited a gradual increase in current, reaching a plateau between 2 and 4 minutes. Here, an optimal accumulation time of 3 minutes yielded higher current responses together with improved reproducibility. These results highlight the importance of tailoring accumulation conditions to the specific electrode material to maximize analytical performance.

Overall, this optimization highlights the importance of carefully adjusting experimental parameters, particularly the nanomaterial type, concentration, and accumulation time, to achieve reliable and sensitive electrochemical monitoring of SMX. Furthermore, the findings reinforce the potential of nanomaterial-based inks to enhance the sensitivity and reproducibility of electrochemical sensors, consolidating their role as promising platforms for environmental monitoring applications.

3.3. Calibration of the SMX quantification in ultrapure water and synthetic hospital effluent

Linear calibration curves for SMX quantification were obtained using electrodes modified with CNF/CNC and CNT/ChNC inks in ultrapure water (Fig. 4 and Table 2). Despite the GCE/CNT/ChNC showing a better response when the accumulation time was evaluated, at lower concentrations, the GCE/CNF/CNC exhibited superior analytical performance with a broader linear range (1–100 mg L^{-1}) and a lower detection limit (LOD) of 0.17 mg L^{-1}. This enhanced sensitivity is likely attributed to favorable interactions between SMX molecules and the nanostructured electrode surface, promoted by the physicochemical properties of type II CNCs and/or CNFs. Based on these results, the GCE/CNF/CNC at 0.4 g L^{-1} and an optimized accumulation time of 1 minute was selected for further evaluation in a synthetic hospital effluent matrix. This step was designed to assess sensor robustness under more complex and realistic conditions. Remarkably, despite the transition from ultrapure water to a synthetic hospital

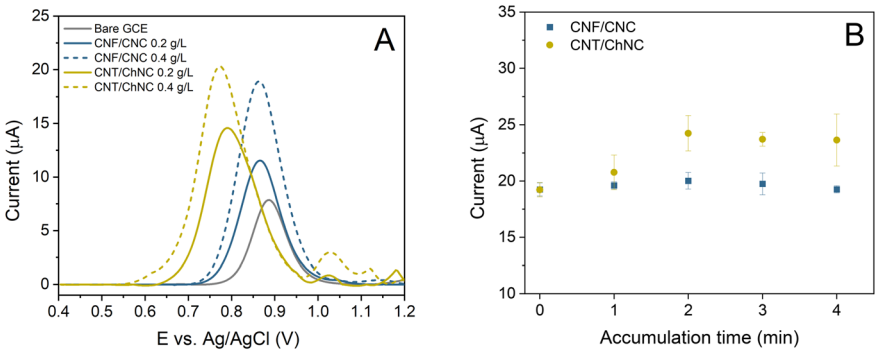

Fig. 3 (A) Differential pulse voltammetry (DPV) of 100 mg L^{-1} SMX in 0.1 M PBS + 0.1 M KCl using electrodes modified with CNM/NB inks at two CNM concentrations (solid line: 0.2 g L^{-1}; dotted line: 0.4 g L^{-1}). The bare GCE is shown as a black solid line for reference. (B) Influence of accumulation time on peak current for 100 mg L^{-1} SMX, CNM/NB concentration: 0.4 g L^{-1} (n = 3).

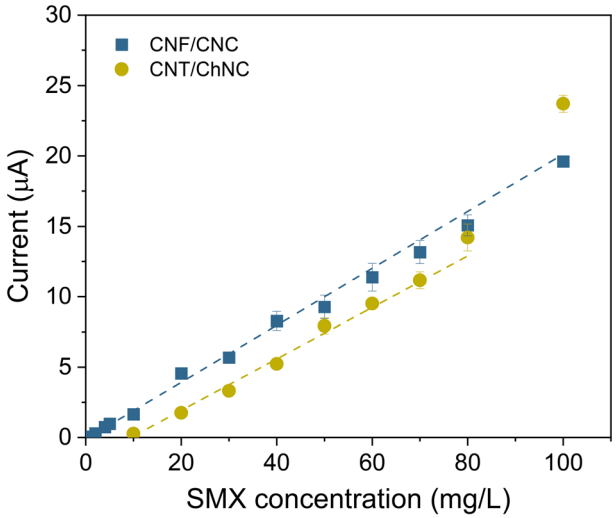

Fig. 4 Calibration curves for SMX quantification with different electrodes in 0.1 M PBS + 0.1 M KCl as a supporting electrolyte. SMX peak current *versus* concentration using electrodes modified with CNF/CNC (0.4 g L^{-1}, 1 min accumulation) and CNT/ChNC (0.4 g L^{-1}, 3 min accumulation) (n = 3).

effluent, the LOD remained unchanged (Table 2). Although the linear range is shorter than that observed in ultrapure water, mainly due to matrix effects, it fully covers the concentration levels typically reported for hospital and pharmaceutical effluents, and is therefore fully compatible with the intended application of the sensor as a process-monitoring tool. This demonstrates that the GCE/CNF/CNC retains its analytical performance even in the presence of competing matrix components. A slight change in the slope of the calibration curve was observed in the synthetic hospital wastewater, likely reflecting interactions between SMX and matrix constituents or minor alterations in the electrode surface environment. Nonetheless, the method delivered consistent detection capabilities, underscoring the reliability of the CNF/CNC-based sensor.

Overall, these findings highlight the relevance of validating electrochemical sensors under environmentally relevant conditions. The CNF/CNC hybrid combines sensitivity, robustness, and reproducibility, making it a strong candidate for practical applications in water quality monitoring and environmental analysis.

SMX, as a pharmaceutical, is typically analyzed in biological or pharmaceutical samples and, to a lesser extent, in water matrices. Table 3 presents some carbon-based sensors developed over the last five years for electrochemical monitoring of SMX in water matrices. The GCE/CNF/CNC electrode developed in this work demonstrated competitive electroanalytical performance compared to previously reported sensors for the detection of SMX in various aqueous matrices. Although its detection limit (0.170 mg L^{-1}) was higher than that of other nanomaterial-based electrodes, its performance must be evaluated in consideration of the application context. Indeed, several highly sensitive systems were validated under relatively controlled conditions, whereas the present electrode was tested in more complex matrices, such as synthetic hospital effluents, which pose an additional challenge due to the presence of interfering substances. Another relevant aspect is the wide linear range obtained (1–100 mg L^{-1}), which surpasses that of several reference sensors. Although these sensors achieve lower detection limits, their quantification ranges are more restricted. This behavior suggests that the GCE/CNF/CNC is a particularly suitable alternative for monitoring moderate to high concentrations of SMX in contaminated water, a common scenario in hospital discharges or urban effluents. Finally, the integration of CNFs and CNCs on the surface of the GCE appears to contribute not only to the sensor's good stability but also to its reproducibility in media with high ionic charge. These results position the system as a balanced proposal between robustness in real matrices and a reliable electrochemical response, albeit with lower sensitivity than other sensors based on metal oxide hybrids or 2D materials.

3.4. Validation of the new electrochemical sensor: monitoring SMX degradation during the application of the solar photo-Fenton process in a pilot-scale raceway pond reactor

The proposed electrochemical sensor was validated by monitoring SMX degradation in synthetic hospital effluent through the solar photo-Fenton process at neutral pH. Experiments were conducted in a pilot-scale raceway pond reactor under natural solar irradiation, utilizing H_2O_2 (1.5 mM) as the oxidant and Fe^{3+}-EDDS (0.10 mM, 1 : 1 molar ratio) as the iron complexing agent to facilitate operation under circumneutral conditions. Two initial SMX concentrations (5 and 10 mg L^{-1}) were tested, and the degradation process was monitored using both UHPLC-DAD, as a reference method, and electrochemical analysis with GCE/CNF/CNC (0.4 g L^{-1}, 1 min accumulation time).

To evaluate whether H_2O_2 and Fe^{3+}-EDDS could interfere with the SMX voltammetric response, the individual electrochemical behavior of both was investigated in the supporting electrolyte (Fig. S3). The results show that H_2O_2 does not exhibit an electroactive signal in the potential

Table 2 Calibration results for the two optimized electrochemical sensor systems in ultrapure water and synthetic hospital wastewater

Electrode	Sample	Linear range (mg L^{-1})	Linear fit equation	R^2	LOD (mg L^{-1})
CNF/CNC	Milli-Q water	1–100	$y = 0.2024 \cdot x - 0.125$	0.994	0.17
CNT/ChNC		10–80	$y = 0.1829 \cdot x - 1.735$	0.993	3.53
CNF/CNC	Synthetic hospital wastewater	1–30	$y = 0.1222 \cdot x - 0.111$	0.999	0.22

Table 3 Carbon-based sensors for the electrochemical detection of SMX in water matrices (2020–2025)

Electrode	Technique	E (V) *vs.* Ag/AgCl	Supporting electrolyte	Linear range (mg L^{-1})	LOD (mg L^{-1})	Water sample	Ref.
GCE/GO/ZnO	DPV	0.85	0.1 M PBS (pH 5.5)	0.03–0.38	0.007	Wastewater treatment plant	53
GCE/TFAB-COF@PANI	DPV	0.86	0.1 M PBS (pH 6.5)	0.25–114	0.027	Tap water, river water	54
GCE/Au-PCMs/Bi_2S_3	DPV	1.1	0.05 M PBS (pH 3.0)	0.001–63.2	0.002	River water, tap water	55
GCE/GR-ZnO	DPV	0.85	0.1 M PBS (pH 7.0)	0.25–10.1	0.101	Tap water, lake water	56
SPCE	DPV	0.78	0.04 M BR (pH 3.0)	1.67–24.4	0.501	Distilled water, tap water, and synthetic hospital wastewater	57
SPCE	DPV	0.78	0.1 M ABS (pH 5.5)	0.05–6	0.015	Tap water	58
SPCE	DPV	0.74	0.1 M tris–HCl (pH 7.0)	0.4–53.8	0.109	River water	59
WP/SHL-GP	DPV	0.71	0.1 M BR (pH 7.0)	1.27–25.3	0.101	Well water, tap water	60
SPCE/rGNR	DPV	0.70	0.1 M PBS (pH 7.0)	0.25–2.53	0.023	Tap water	61
CPE/BN-Fe_3O_4-Pd	DPV	0.94	0.1 M PBS (pH 7.0)	0.005–106.4	0.002	Tap water, river water	62
GCE/g-C_3N_4/CDs	DPV	0.65	0.1 M PBS (pH 5.0)	0.076–0.279	0.025	Tap water, effluent water	63
GCE/MXOF	SWV	0.36	0.1 M PBS (pH 7.0)	25.3–253.3	0.039	Tap water	64
GCE/CNF/CNC	DPV	0.86	0.1 M PBS + 0.1 M KCl (pH 7.0)	1–100 1–30	0.170 0.220	Milli-Q water Synthetic hospital wastewater	This work

GCE: glassy carbon electrode; GO/ZnO: graphene oxide/zinc oxide; TFAB-COF@PANI: covalent organic framework on polyaniline; Au-PCM/Bi_2S_3: gold nanoparticles–porous carbon microsheets/Bi_2S_3; GR: graphene; SPCE: screen-printed carbon electrode; WP/SHL-GP: waterproof paper/shellac-graphene; rGNR: reduced graphene nanoribbons; CPE/BN: carbon paste electrode/boron nitride; g-C_3N_4/CDs: graphitic carbon nitride/carbon dots; MXOF: MXene/metal–organic framework; PBS: phosphate buffer solution; ABS: acetate buffer solution; BR: Britton–Robinson buffer.

window used for SMX detection, and therefore does not contribute to the current or interfere with the analytical signal. In the case of Fe^{3+}-EDDS, a reversible redox signal is observed, attributable to the Fe^{3+}/Fe^{2+} couple. However, this signal appears at potentials different from those at which SMX electrochemically oxidizes under the DPV conditions. Based on this, neither species is considered to interfere with SMX detection.

The solar photo-Fenton treatment mediated by Fe^{3+}-EDDS showed the characteristic pollutant removal profile (Fig. 5A). During the first 20 minutes, rapid degradation was observed, associated with the presence of Fe^{3+}-EDDS in solution and its photolysis-driven interaction with H_2O_2, resulting in the generation of hydroxyl radicals (HO·). Near-complete Fe^{3+}-EDDS depletion was reached within ~20 minutes, primarily due to direct photolysis and the reaction with the produced radicals (Fig. 5B). The consumption of Fe^{3+}-EDDS was accompanied by a rapid decrease in H_2O_2 concentration, which subsequently slowed down after complex depletion. SMX removal followed a parallel trend, characterized by an initial sharp decline within the first 20 minutes, followed by stabilization, consistent with the cessation of radical generation upon Fe^{3+}-EDDS consumption (Fig. 5A).

A comparison of UHPLC-DAD and electrochemical analysis results for the 10 mg L^{-1} SMX experiment revealed a highly consistent degradation trend (Fig. 5A). The electrochemical sensor successfully captured the characteristic profile of SMX degradation, with an initial rapid decrease followed by stabilization after 15 minutes. Minor discrepancies were observed during the early stages, particularly at t = 0, but overall, the sensor exhibited excellent performance for quantifying SMX concentrations between 5 and 1 mg L^{-1}. Interestingly, for the 5 mg L^{-1} experiment, the initial deviation between the electrochemical and UHPLC-DAD values at t = 0 was notably smaller than in the 10 mg L^{-1} case. However, due to the rapid degradation of SMX

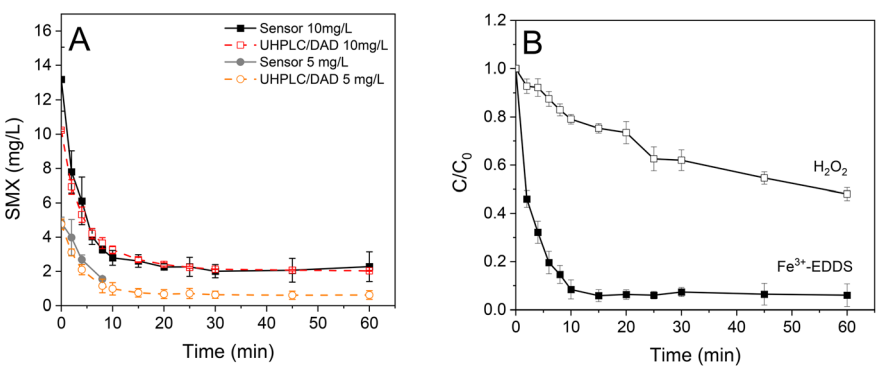

Fig. 5 (A) SMX concentration profiles measured using the electrochemical sensor GCE/CNF/CNC (0.4 g L^{-1}, 1 min accumulation) compared with UHPLC-DAD; (B) normalized decomposition profiles of Fe^{3+}-EDDS (catalyst) and H_2O_2 (oxidant agent) showing the reaction dynamics during the solar photo-Fenton process.

under these conditions, concentrations fell below the sensor's LOD within 10 minutes, preventing further electrochemical monitoring.

These findings underscore the robustness and applicability of the CNF/CNC-modified sensor for real-time SMX quantification, even in complex matrices, and highlight its potential for monitoring SMX removal during advanced wastewater treatment processes, where degradation by-products may interfere with conventional methods.

To further validate the performance of the proposed sensor, an in-depth statistical comparison with UHPLC-DAD measurements was conducted, including correlation analysis, linear regression, and Bland–Altman evaluation.[65] The resulting parameters are summarized in Table 4 and correspond to the degradation experiments shown in Fig. 5.

In both experiments, a strong linear correlation was observed between the electrochemical sensor measurements and reference UHPLC data. For the experiment starting with 10 mg L^{-1} SMX, the Pearson correlation coefficient was r = 0.997, indicating an excellent relationship. The regression slope (m = 0.719) indicated that the sensor systematically underestimates concentrations relative to UHPLC at higher levels. In contrast, for the experiment with 5 mg L^{-1} SMX, the correlation remained strong (r = 0.974), with a slope close to unity (m = 1.041), suggesting good proportionality between methods.

The agreement between the two techniques was further evaluated using Bland–Altman analysis. For the 10 mg L^{-1} experiment, the mean difference was +0.71 mg L^{-1}, with limits of agreement (LoA) from −1.25 mg L^{-1} to +2.68 mg L^{-1}. This indicates a minor positive bias of the electrochemical sensor relative to UHPLC, though the variability remained within an acceptable range for environmental monitoring applications.

In contrast, for $C_0 \approx 5$ mg L^{-1}, the mean difference was +0.47 mg L^{-1}, with a narrower LoA value ranging from −0.22 mg L^{-1} to +1.16 mg L^{-1}. Although the absolute dispersion was lower than in the 10 mg L^{-1} experiment, the relative impact of these deviations becomes more significant when working close to the detection limit or within sensitive concentration ranges. This is consistent with the lower measured concentrations and highlights the importance of carefully addressing sensitivity thresholds.

Table 4 Statistical analysis comparing the electrochemical sensor and UHPLC/DAD measurements

SMX (mg L^{-1})	10	5
	Pearson coefficient	
r	0.997	0.974
	Linear regression	
Slope	0.719	1.041
Intercept	0.538	−0.603
	Bland–Altman plot	
Mean difference (sensor − UHPLC)	0.71	0.47
SD	0.0036	0.0041
Upper LoA (mean + 1.96 SD)	2.67	1.16
Lower LoA (mean − 1.96 SD)	−1.24	−0.22

Overall, these results confirm that the electrochemical sensor demonstrates strong correlation and agreement with the reference chromatographic method across both tested concentration ranges. Nevertheless, the detailed analysis reveals that the sensor performance is more robust in the mid-to-high concentration range ($C_0 \approx 10$ mg L^{-1}). At lower concentrations ($C_0 \approx 5$ mg L^{-1}), additional measures, such as careful calibration, validation of the detection limit, and consideration of potential matrix effects, become increasingly critical to ensure reliable quantification.

Although no isolated interference tests were performed, the selectivity of the proposed sensor was assessed at an operational level, in line with its intended application as a process-monitoring tool. Rather than relying on molecular recognition mechanisms, the sensor performance was evaluated through direct comparison with UHPLC-DAD in a complex synthetic effluent representative of hospital wastewater.

This matrix contained typical inorganic ions (*e.g.*, Ca^{2+}, Mg^{2+}, K^{+}, Na^{+}, phosphate, and bicarbonate) and organic constituents (*e.g.*, humic substances, surfactants, and peptones), all of which may act as potential interferents in electrochemical measurements. Despite this chemical complexity, the strong agreement observed between the electrochemical measurements and UHPLC-DAD indicates that, under the selected experimental conditions and within the investigated concentration range (mg L^{-1}), the electrochemical response is predominantly governed by SMX.

This level of operational selectivity is appropriate for monitoring SMX concentration dynamics during controlled wastewater treatment processes and supports the sensor's applicability for process monitoring in high-load effluents, rather than for untargeted multi-analyte detection.

It is worth noting that, across all published studies, SMX detection is performed using standard addition. In contrast, this work directly detects the concentration from the pilot plant and then extrapolates it from the calibration curve.

4. Conclusion

The real-world applicability of the proposed electrochemical sensor was demonstrated by monitoring SMX degradation during a solar photo-Fenton process operated at circumneutral pH in a pilot-scale raceway pond reactor. This validation under operationally relevant conditions represents a key contribution of the present study, as electrochemical sensors are still rarely evaluated beyond controlled laboratory environments in the context of wastewater treatment. Despite minor discrepancies observed during the initial stages of the treatment, the electrochemical sensor reliably reproduced the SMX degradation profiles obtained by UHPLC-DAD, particularly within the 1–5 mg L^{-1} concentration range. The strong agreement between the two analytical approaches confirms the robustness and reliability of the sensor for tracking concentration dynamics during AOPs, even in complex matrices containing oxidants, metal complexes, and reaction by-products.

Importantly, the sensor's analytical performance should be interpreted in light of its intended application domain. Rather than targeting ultra-trace detection, the sensor was specifically designed for process monitoring in high-load effluents, such as hospital and pharmaceutical wastewater, where SMX concentrations typically fall within the mg L^{-1} range. Within this context, the sensor exhibits a wide linear response, good reproducibility, and sufficient sensitivity to provide timely and actionable information for process control and optimization. While further improvements would be required to extend its applicability toward ultra-trace analysis in urban wastewater, this limitation does not compromise its suitability for the targeted monitoring scenarios addressed in this work. From a materials perspective, the use of eco-friendly, fully water-processed hybrid inks based on carbon nanomaterials and nanostructured biopolymers represents a sustainable alternative to conventional electrode modification strategies (typically relying on organic solvents or surfactants). Among the tested formulations, the CNF/CNC-based ink provided the most suitable performance for SMX monitoring, combining a stable electrochemical response with robustness under complex operating conditions.

Overall, this study demonstrates the potential of nanomaterial-based electrochemical sensors as cost-effective, portable, and environmentally friendly tools for monitoring and controlling advanced wastewater treatment processes. By validating sensor performance under near-real operational conditions and at the pilot scale, this work helps to bridge the often-overlooked gap between laboratory-scale sensor development and practical implementation in wastewater treatment systems.

Future research will focus on improving sensor robustness and operational selectivity, extending validation to real, complex wastewater matrices, and integrating the sensing platform with miniaturized, disposable electrodes, such as screen-printed electrodes. These developments will facilitate large-scale, on-site, near-real-time monitoring of water quality, supporting the deployment of electrochemical sensing technologies in advanced, decentralized wastewater treatment applications.

Conflicts of interest

There are no conflicts to declare.

Note after first publication

This article replaces the version published on 06 Mar 2026, which contained incorrect peak labels in Fig. 1B. The Royal Society of Chemistry apologises for any confusion.

Data availability

The data supporting this article have been included as part of the supplementary information (SI).

Supplementary information is available. See DOI: https://doi.org/10.1039/d6en00086j.

Acknowledgements

This work was supported by the Spanish MCIN/AEI and "ERDF A way of making Europe" [PID2022-139671OB-I00, PID2023-147116OB-I00], Gobierno de Aragón (DGA) [T03_23R (Grupos de Investigación Reconocidos), CUS/581/2020 (PhD contract) (V. C.), CUS/1668/2022 (research stay) (V. C.), R&D&I projects in priority lines and of a multidisciplinary nature (project grant PROY_T41_24)], ANID-FONDECYT [no. 1231258 (P. S.-R.), no. 11240700 (C. J. V.)], and ANID-FONDAP [No. 1523A0006 (S. M.-C.; A. C.)]. Dr. Miralles-Cuevas would like to acknowledge the RYC2023-042474-I grant, funded by MCIU/AEI/10.13039/501100011033 and the FSE+. SEM images were obtained thanks to the project supported by the "Plan de Fortalecimiento de Universidades Estatales 2019, UTM1999, MINEDUC" (Chile). A. Cabrera would like to acknowledge CNS2024-154926, supported by MICIU/AEI/10.13039/501100011033.

References

1 J. L. Wilkinson, *et al.*, Pharmaceutical pollution of the world's rivers, *Proc. Natl. Acad. Sci. U. S. A.*, 2022, **119**, e2113947119, DOI: 10.1073/pnas.2113947119.
2 C. Peña-Guzmán, S. Ulloa-Sánchez, K. Mora, R. Helena-Bustos, E. Lopez-Barrera, J. Alvarez and M. Rodriguez-Pinzón, Emerging pollutants in the urban water cycle in Latin America: A review of the current literature, *J. Environ. Manage.*, 2019, **237**, 408–423, DOI: 10.1016/j.jenvman.2019.02.100.
3 Directive (EU) 2024/3019 of the European Parliament and of the Council of 12 December 2024 concerning urban wastewater treatment, 2024, http://data.europa.eu/eli/dir/2024/3019/oj.
4 B. Coulibaly, E. J. Pastor-López, A. Diawara, F. B. Savane, M. Escolà-Casas, V. Matamoros and S. Ba, Occurrence of antibiotics in hospital wastewater effluents discharged into the Niger River in Bamako, Mali. Risk assessment and solutions, *Environ. Pollut.*, 2025, **371**, 125912, DOI: 10.1016/j.envpol.2025.125912.
5 K. V. Thomas, C. Dye, M. Schlabach and K. H. Langford, Source to sink tracking of selected human pharmaceuticals from two Oslo city hospitals and a wastewater treatment works, *J. Environ. Monit.*, 2007, **9**, 1410–1418, DOI: 10.1039/B709745J.
6 M. J. Gómez, M. Petrović, A. R. Fernández-Alba and D. Barceló, Determination of pharmaceuticals of various therapeutic classes by solid-phase extraction and liquid chromatography-tandem mass spectrometry analysis in hospital effluent wastewaters, *J. Chromatogr. A*, 2006, **1114**, 224–233, DOI: 10.1016/j.chroma.2006.02.038.
7 F. Z. Deedat, A. M. Faya, B. P. Gumbi, D. M. G. Johnston, R. Karpoormath and S. Y. Essack, The association between antibiotic use in hospitals and residual antibiotic concentrations in hospital effluents: a pilot study, *JAC Antimicrob. Resist.*, 2025, **7**, dlaf070, DOI: 10.1093/jacamr/dlaf070.

8 P. Kovalakova, L. Cizmas, T. J. McDonald, B. Marsalek, M. Feng and V. K. Sharma, Occurrence and toxicity of antibiotics in the aquatic environment: A review, *Chemosphere*, 2020, **251**, 126351, DOI: 10.1016/j.chemosphere.2020.126351.
9 Commission Implementing Decision (EU) 2020/1161, 2020.
10 Commission Implementing Decision (EU) 2022/1307, 2022.
11 M. Xu, J. Li, Y. Yan, X. Zhao, J. Yan, Y. Zhang, B. Lai, X. Chen and L. Song, Catalytic degradation of sulfamethoxazole through peroxymonosulfate activated with expanded graphite loaded CoFe2O4 particles, *Chem. Eng. J.*, 2019, **369**, 403–413, DOI: 10.1016/j.cej.2019.03.075.
12 Y. Li, J. Li, Y. Pan, Z. Xiong, G. Yao, R. Xie and B. Lai, Peroxymonosulfate activation on FeCo2S4 modified g-C3N4 (FeCo2S4-CN): Mechanism of singlet oxygen evolution for nonradical efficient degradation of sulfamethoxazole, *Chem. Eng. J.*, 2020, **384**, 123361, DOI: 10.1016/j.cej.2019.123361.
13 Z. Wang, J. Wang, B. Xiong, F. Bai, S. Wang, Y. Wan, L. Zhang, P. Xie and M. R. Wiesner, Application of Cobalt/Peracetic Acid to Degrade Sulfamethoxazole at Neutral Condition: Efficiency and Mechanisms, *Environ. Sci. Technol.*, 2020, **54**, 464–475, DOI: 10.1021/acs.est.9b04528.
14 K. Kowalska, M. Roccamante, A. C. Reina, P. Plaza-Bolaños, I. Oller and S. Malato, Pilot-scale removal of microcontaminants by solar-driven photo-Fenton in treated municipal effluents: Selection of operating variables based on lab-scale experiments, *J. Environ. Chem. Eng.*, 2021, **9**, 104788, DOI: 10.1016/j.jece.2020.104788.
15 J. Herrera-Muñoz, A. Cabrera-Reina, S. Miralles-Cuevas, S. Piña and R. Salazar-González, Simultaneous degradation of contaminants of emerging concern and disinfection by solar photoelectro-Fenton process at circumneutral pH in a solar electrochemical raceway pond reactor, *Chemosphere*, 2023, **341**, 139978, DOI: 10.1016/j.chemosphere.2023.139978.
16 R. Kumar, M. Qureshi, D. K. Vishwakarma, N. Al-Ansari, A. Kuriqi, A. Elbeltagi and A. Saraswat, A review on emerging water contaminants and the application of sustainable removal technologies, *Case Stud. Chem. Environ. Eng.*, 2022, **6**, 100219, DOI: 10.1016/j.cscee.2022.100219.
17 A. Saravanan, V. C. Deivayanai, P. S. Kumar, G. Rangasamy, R. V. Hemavathy, T. Harshana, N. Gayathri and K. Alagumalai, A detailed review on advanced oxidation process in treatment of wastewater: Mechanism, challenges and future outlook, *Chemosphere*, 2022, **308**, 136524, DOI: 10.1016/j.chemosphere.2022.136524.
18 S. Campos, J. Lorca, J. Vidal, W. Calzadilla, C. Toledo-Neira, M. Aranda, S. Miralles-Cuevas, A. Cabrera-Reina and R. Salazar, Removal of contaminants of emerging concern by solar photo electro-Fenton process in a solar electrochemical raceway pond reactor, *Process Saf. Environ. Prot.*, 2023, **169**, 660–670, DOI: 10.1016/j.psep.2022.11.033.
19 P. Soriano-Molina, S. Miralles-Cuevas, B. Esteban García, P. Plaza-Bolaños and J. A. Sánchez Pérez, Two strategies of solar photo-Fenton at neutral pH for the simultaneous disinfection and removal of contaminants of emerging concern. Comparative assessment in raceway pond reactors, *Catal. Today*, 2021, **361**, 17–23, DOI: 10.1016/j.cattod.2019.11.028.
20 S. Miralles-Cuevas, I. Oller, A. Agüera, J. A. Sánchez Pérez and S. Malato, Strategies for reducing cost by using solar photo-Fenton treatment combined with nanofiltration to remove microcontaminants in real municipal effluents: Toxicity and economic assessment, *Chem. Eng. J.*, 2017, **318**, 161–170, DOI: 10.1016/j.cej.2016.06.031.
21 J. A. Sánchez Pérez, I. M. Román Sánchez, I. Carra, A. Cabrera Reina, J. L. Casas López and S. Malato, Economic evaluation of a combined photo-Fenton/MBR process using pesticides as model pollutant. Factors affecting costs, *J. Hazard. Mater.*, 2013, **244–245**, 195–203, DOI: 10.1016/j.jhazmat.2012.11.015.
22 L. Rizzo, W. Gernjak, P. Krzeminski, S. Malato, C. S. McArdell, J. A. S. Perez, H. Schaar and D. Fatta-Kassinos, Best available technologies and treatment trains to address current challenges in urban wastewater reuse for irrigation of crops in EU countries, *Sci. Total Environ.*, 2020, **710**, 136312, DOI: 10.1016/j.scitotenv.2019.136312.
23 E. Gualda-Alonso, P. Soriano-Molina, J. L. Casas López, J. L. García Sánchez, P. Plaza-Bolaños, A. Agüera and J. A. Sánchez Pérez, Large-scale raceway pond reactor for CEC removal from municipal WWTP effluents by solar photo-Fenton, *Appl. Catal., B*, 2022, **319**, 121908, DOI: 10.1016/j.apcatb.2022.121908.
24 E. Gualda-Alonso, N. Pichel, P. Soriano-Molina, E. Olivares-Ligero, F. X. Cadena-Aponte, A. Agüera, J. A. Sánchez Pérez and J. L. Casas López, Continuous solar photo-Fenton for wastewater reclamation in operational environment at demonstration scale, *J. Hazard. Mater.*, 2023, **459**, 132101, DOI: 10.1016/j.jhazmat.2023.132101.
25 D. Rodríguez-García, P. Soriano-Molina, J. L. Guzmán Sánchez, J. L. García Sánchez, J. L. Casas López and J. A. Sánchez Pérez, A novel control system approach to enhance the efficiency of solar photo-Fenton microcontaminant removal in continuous flow raceway pond reactors, *Chem. Eng. J.*, 2023, **455**, 140760, DOI: 10.1016/j.cej.2022.140760.
26 Y. Xiangwei, M. Graells, S. Miralles-Cuevas, A. Cabrera-Reina and M. Pérez-Moya, An improved hybrid strategy for online dosage of hydrogen peroxide in photo-Fenton processes, *J. Environ. Chem. Eng.*, 2021, **9**, 105235, DOI: 10.1016/j.jece.2021.105235.
27 X. Yu, A. Cabrera-Reina, M. Graells, S. Miralles-Cuevas and M. Pérez-Moya, Towards an efficient generalization of the online dosage of hydrogen peroxide in photo-fenton process to treat industrial wastewater, *Int. J. Environ. Res. Public Health*, 2021, **18**(24), 13313, DOI: 10.3390/ijerph182413313.
28 C. J. Venegas, L. Rodríguez and P. Sierra-Rosales, Selective Label-Free Electrochemical Aptasensor Based on Carbon Nanotubes for Carbendazim Detection, *Chemosensors*, 2023, **11**(2), 117, DOI: 10.3390/chemosensors11020117.
29 R. Sivaranjanee, P. Senthil Kumar, R. Saravanan and M. Govarthanan, Electrochemical sensing system for the analysis of emerging contaminants in aquatic environment: A review, *Chemosphere*, 2022, **294**, 133779, DOI: 10.1016/j.chemosphere.2022.133779.

30 C. J. Venegas, S. Bollo and P. Sierra-Rosales, Carbon-Based Electrochemical (Bio)sensors for the Detection of Carbendazim: A Review, *Micromachines*, 2023, **14**(9), 1752, DOI: 10.3390/mi14091752.
31 D. Jović, V. Jaćević, K. Kuča, I. Borišev, J. Mrdjanovic, D. Petrovic, M. Seke and A. Djordjevic, The puzzling potential of carbon nanomaterials: General properties, application, and toxicity, *Nanomaterials*, 2020, **10**, 1–30, DOI: 10.3390/nano10081508.
32 V. Schroeder, S. Savagatrup, M. He, S. Lin and T. M. Swager, Carbon nanotube chemical sensors, *Chem. Rev.*, 2019, **119**, 599–663, DOI: 10.1021/acs.chemrev.8b00340.
33 S. Lu, B. N. Smith, H. Meikle, M. J. Therien and A. D. Franklin, All-Carbon Thin-Film Transistors Using Water-Only Printing, *Nano Lett.*, 2023, **23**, 2100–2106, DOI: 10.1021/acs.nanolett.2c04196.
34 J. M. González-Domínguez, A. Baigorri, M. Álvarez-Sánchez, E. Colom, B. Villacampa, A. Ansón-Casaos, E. García-Bordejé, A. M. Benito and W. K. Maser, Waterborne graphene-and nanocellulose-based inks for functional conductive films and 3d structures, *Nanomaterials*, 2021, **11**(6), 1435, DOI: 10.3390/nano11061435.
35 Y. He, X. Lin, Y. Feng, B. Luo and M. Liu, Carbon Nanotube Ink Dispersed by Chitin Nanocrystals for Thermoelectric Converter for Self-Powering Multifunctional Wearable Electronics, *Adv. Sci.*, 2022, **9**, 2204675, DOI: 10.1002/advs.202204675.
36 J. M. González-Domínguez, A. Ansón-Casaos, L. Grasa, L. Abenia, A. Salvador, E. Colom, J. E. Mesonero, J. E. García-Bordejé, A. M. Benito and W. K. Maser, Unique Properties and Behavior of Nonmercerized Type-II Cellulose Nanocrystals as Carbon Nanotube Biocompatible Dispersants, *Biomacromolecules*, 2019, **20**, 3147–3160, DOI: 10.1021/acs.biomac.9b00722.
37 V. Calvo, A. J. Paleo, J. M. González-Domínguez, E. Muñoz, B. Krause, P. Pötschke, W. K. Maser and A. M. Benito, The aqueous processing of carbon nanofibers via cellulose nanocrystals as a green path towards e-textiles with n-type thermoelectric behaviour, *Carbon*, 2024, **217**, 118640, DOI: 10.1016/j.carbon.2023.118640.
38 S. Dortez, T. Sierra, M. Á. Álvarez-Sánchez, J. M. González-Domínguez, A. M. Benito, W. K. Maser, A. G. Crevillen and A. Escarpa, Effect of nanocellulose polymorphism on electrochemical analytical performance in hybrid nanocomposites with non-oxidized single-walled carbon nanotubes, *Microchim. Acta*, 2022, **189**, 62, DOI: 10.1007/s00604-021-05161-w.
39 V. Calvo, L. Fuentes, D. Berdejo, J. M. González-Domínguez, W. K. Maser and A. M. Benito, Oil-in-Water Pickering Emulsions Stabilized with Nanostructured Biopolymers: A Venue for Templating Bacterial Cellulose, *Int. J. Mol. Sci.*, 2023, **24**, 13141, DOI: 10.3390/ijms241713141.
40 A. Narkevicius, L. M. Steiner, R. M. Parker, Y. Ogawa, B. Frka-Petesic and S. Vignolini, Controlling the Self-Assembly Behavior of Aqueous Chitin Nanocrystal Suspensions, *Biomacromolecules*, 2019, **20**, 2830–2838, DOI: 10.1021/acs.biomac.9b00589.
41 G. Sèbe, F. Ham-Pichavant, E. Ibarboure, A. L. C. Koffi and P. Tingaut, Supramolecular Structure Characterization of Cellulose II Nanowhiskers Produced by Acid Hydrolysis of Cellulose I Substrates, *Biomacromolecules*, 2012, **13**, 570–578, DOI: 10.1021/bm201777j.
42 V. Calvo, C. Martínez-Barón, B. Vazquez-Conejo, A. Dominguez-Alfaro, A. J. Paleo, B. Villacampa, A. Ansón-Casaos, W. K. Maser, A. M. Benito and J. M. Gonzalez-Dominguez, Carbon nanomaterials-based inks and electrodes using chitin nanocrystals, *ACS Sustainable Chem. Eng.*, 2024, **12**(43), 15980–15990, DOI: 10.1021/acssuschemeng.4c05253.
43 V. Calvo, M. Á. Álvarez Sánchez, L. Güemes, C. Martínez-Barón, S. Baúlde, A. Criado, J. M. González-Domínguez, W. K. Maser and A. M. Benito, Preparation of Cellulose Nanocrystals: Controlling the Crystalline Type by One-Pot Acid Hydrolysis, *ACS Macro Lett.*, 2023, **12**, 152–158, DOI: 10.1021/acsmacrolett.2c00705.
44 J. D. Goodrich and W. T. Winter, α-Chitin Nanocrystals Prepared from Shrimp Shells and Their Specific Surface Area Measurement, *Biomacromolecules*, 2007, **8**, 252–257, DOI: 10.1021/bm0603589.
45 R. Zhang, S. Vigneswaran, H. Ngo and H. Nguyen, A submerged membrane hybrid system coupled with magnetic ion exchange (MIEX®) and flocculation in wastewater treatment, *Desalination*, 2007, **216**, 325–333, DOI: 10.1016/j.desal.2006.11.025.
46 N. Klamerth, S. Malato, A. Agüera, A. Fernández-Alba and G. Mailhot, Treatment of municipal wastewater treatment plant effluents with modified photo-fenton as a tertiary treatment for the degradation of micro pollutants and disinfection, *Environ. Sci. Technol.*, 2012, **46**, 2885–2892, DOI: 10.1021/es204112d.
47 I. De la Obra, L. Ponce-Robles, S. Miralles-Cuevas, I. Oller, S. Malato and J. A. Sánchez Pérez, Microcontaminant removal in secondary effluents by solar photo-Fenton at circumneutral pH in raceway pond reactors, *Catal. Today*, 2017, **287**, 10–14, DOI: 10.1016/j.cattod.2016.12.028.
48 S. Miralles-Cuevas, I. Oller, J. A. S. Pérez and S. Malato, Application of solar photo-Fenton at circumneutral pH to nanofiltration concentrates for removal of pharmaceuticals in MWTP effluents, *Environ. Sci. Pollut. Res.*, 2015, **22**, 846–855, DOI: 10.1007/s11356-014-2871-2.
49 A. Cabrera-Reina, S. Miralles-Cuevas, J. A. Sánchez Pérez and R. Salazar, Application of solar photo-Fenton in raceway pond reactors: A review, *Sci. Total Environ.*, 2021, **800**, 149653, DOI: 10.1016/j.scitotenv.2021.149653.
50 Y. Wu, M. Brigante, W. Dong, P. De Sainte-Claire and G. Mailhot, Toward a better understanding of Fe(III)-EDDS photochemistry: Theoretical stability calculation and experimental investigation of 4- tert -butylphenol degradation, *J. Phys. Chem. A*, 2014, **118**, 396–403, DOI: 10.1021/jp409043e.
51 B. Patel, *Electrochemistry for Bioanalysis*, Elsevier, 2020, DOI: 10.1016/c2019-0-03108-1.

52 P. Sampathkumar, J. Muthuthivya, T. Nandhaganesh, D. Soundarya and C. Suresh, Sensing technologies for agroenvironment toward sustainable human healthcare, in *Health and Environmental Applications of Biosensing Technologies: Clinical and Allied Health Science Perspective*, Elsevier, 2023, pp. 245–266, DOI: 10.1016/B978-0-443-19039-1.00012-2.

53 P. Senthil Kumar, B. S. Sreeja, K. Krishna Kumar and G. Padmalaya, Static and dynamic analysis of sulfamethoxazole using GO/ZnO modified glassy carbon electrode by differential pulse voltammetry and amperometry techniques, *Chemosphere*, 2022, **302**, 134926, DOI: 10.1016/j.chemosphere.2022.134926.

54 Z. Pan, Y. Wei, H. Guo, B. Liu, L. Sun, Z. Lu, X. Wei, H. Zhang, Y. Chen and W. Yang, Sensitive detection of sulfamethoxazole by an electrochemical sensing platform with a covalent organic framework in situ grown on polyaniline, *Microporous Mesoporous Mater.*, 2023, **348**, 112409, DOI: 10.1016/j.micromeso.2022.112409.

55 R. Nehru, B. Senthil Kumar, C. W. Chen and C. Di Dong, Surface modification of Au nanoparticles with porous carbon microsheets/Bi2S3 for enhanced electrochemical monitoring of hazardous sulfamethoxazole, *J. Environ. Chem. Eng.*, 2024, **12**, 114814, DOI: 10.1016/j.jece.2024.114814.

56 X. Yue, Z. Li and S. Zhao, A new electrochemical sensor for simultaneous detection of sulfamethoxazole and trimethoprim antibiotics based on graphene and ZnO nanorods modified glassy carbon electrode, *Microchem. J.*, 2020, **159**, 105440, DOI: 10.1016/j.microc.2020.105440.

57 S. Caruncho-Pérez, N. Bernárdez, M. Pazos, M. Á. Sanromán and E. González-Romero, Voltammetric methodology for the quality control and monitoring of sulfamethoxazole removal from water, *Talanta*, 2025, **284**, 127255, DOI: 10.1016/j.talanta.2024.127255.

58 E. Alberto, J. Bastos-Arrieta, C. Pérez-Ràfols, N. Serrano, M. Silvia Díaz-Cruz and J. Manuel Díaz-Cruz, Voltammetric determination of sulfamethoxazole using commercial screen-printed carbon electrodes, *Microchem. J.*, 2023, **193**, 109125, DOI: 10.1016/j.microc.2023.109125.

59 J. Huang, J. Bastos-Arrieta, N. Serrano and J. M. Díaz-Cruz, Voltammetric Determination of Salbutamol, Sulfamethoxazole, and Trimethoprim as Anthropogenic Impact Indicators Using Commercial Screen-Printed Electrodes, *Sensors*, 2025, **25**(10), 2998, DOI: 10.3390/s25102998.

60 J. Melo Henrique, J. Rocha Camargo, G. Gabriel de Oliveira, J. Santos Stefano and B. Campos Janegitz, Disposable electrochemical sensor based on shellac and graphite for sulfamethoxazole detection, *Microchem. J.*, 2021, **170**, 106701, DOI: 10.1016/j.microc.2021.106701.

61 T. S. Martins, J. L. Bott-Neto, O. N. Oliveira and S. A. S. Machado, Paper-based electrochemical sensors with reduced graphene nanoribbons for simultaneous detection of sulfamethoxazole and trimethoprim in water samples, *J. Electroanal. Chem.*, 2021, **882**, 114985, DOI: 10.1016/j.jelechem.2021.114985.

62 S. Tajik, H. Beitollahi, M. Shahedi Asl, H. W. Jang and M. Shokouhimehr, BN-Fe3O4-Pd nanocomposite modified carbon paste electrode: Efficient voltammetric sensor for sulfamethoxazole, *Ceram. Int.*, 2021, **47**, 13903–13911, DOI: 10.1016/j.ceramint.2021.01.257.

63 T. H. G. Moundzounga, M. G. Peleyeju, B. O. Orimolade, A. M. Olatunde, W. K. Maboya, S. O. Akpotu, M. M. Chili and M. J. Klink, Voltammetric analysis of As3+ and sulfamethoxazole on an electrode modified with a composite of carbon dots and graphitic carbon nitride, *Int. J. Electrochem. Sci.*, 2025, **20**(3), 100947, DOI: 10.1016/j.ijoes.2025.100947.

64 P. Seyadu Abuthahir, M. Manikandan and E. Manikandan, Electrochemical detection of sulfamethoxazole antibiotics in water using MXene/ZIF-8 composite modified glassy carbon electrode, *npj 2D Mater. Appl.*, 2025, **9**, 42, DOI: 10.1038/s41699-025-00555-3.

65 P. Mishra, C. Pandey, U. Singh, A. Keshri and M. Sabaretnam, Selection of appropriate statistical methods for data analysis, *Ann. Card. Anaesth.*, 2019, **22**, 297–301, DOI: 10.4103/aca.ACA_248_18.